

AD-A 200 937

Technical Report
814

DTIC FILE COPY

Design of a Wafer-Scale Focal Plane Processor

P.C. Trepagnier

15 September 1988

Lincoln Laboratory

MASSACHUSETTS INSTITUTE OF TECHNOLOGY

LEXINGTON, MASSACHUSETTS



Prepared for the Department of the Air Force
under Electronic Systems Division Contract F19628-85-C-0002

Approved for public release; distribution unlimited.

DTIC
ELECTE
DEC 02 1988

S

E

88 12 2 035

The work reported in this document was performed at Lincoln Laboratory, a center for research operated by Massachusetts Institute of Technology, with the support of the Department of the Air Force under Contract F19628-85-C-0002.

This report may be reproduced to satisfy needs of U.S. Government agencies.

The views and conclusions contained in this document are those of the contractor and should not be interpreted as necessarily representing the official policies, either expressed or implied, of the United States Government.

The ESD Public Affairs Office has reviewed this report, and it is releasable to the National Technical Information Service, where it will be available to the general public, including foreign nationals.

This technical report has been reviewed and is approved for publication.

FOR THE COMMANDER

Hugh L. Southall

Hugh L. Southall, Lt. Col., USAF
Chief, ESD Lincoln Laboratory Project Office

Non-Lincoln Recipients

PLEASE DO NOT RETURN

Permission is given to destroy this document
when it is no longer needed.

MASSACHUSETTS INSTITUTE OF TECHNOLOGY
LINCOLN LABORATORY

DESIGN OF A WAFER-SCALE FOCAL PLANE PROCESSOR

P.C. TREPAGNIER
Group 27

TECHNICAL REPORT 814

15 SEPTEMBER 1988

Approved for public release; distribution unlimited.

LEXINGTON

MASSACHUSETTS

ABSTRACT

This report describes a wafer-scale design for an infrared focal plane processor (FPP) to operate in a space environment. The functions of a generic focal plane processor are described, followed by a detailed discussion of a design to be implemented in RVLSI wafer-scale technology for a space-based application. A prototype of this processor (PFPP) will actually be fabricated in rad-hard silicon-on-insulator 3- μ m technology. Finally, the question of reliability is explored, and a philosophy of fault-tolerance is presented which will lead to a reasonable probability of success over a five-year lifetime.

Accession For	
NTIS GRA&I	<input checked="" type="checkbox"/>
DTIC TAB	<input type="checkbox"/>
Unannounced	<input type="checkbox"/>
Justification	
By _____	
Distribution/	
Availability Codes	
Dist	Avail and/or Special
A-1	



TABLE OF CONTENTS

ABSTRACT	iii
LIST OF ILLUSTRATIONS	vi
LIST OF TABLES	vii
ACKNOWLEDGEMENTS	ix
1. INTRODUCTION	1
1.1 Scanning Arrays	1
1.2 Focal Plane Processor	1
1.3 Fault Tolerance	2
1.4 Wafer Scale Integration	3
1.5 Organization of Report	3
2. DESIGN OF A PROTOTYPE FOCAL PLANE PROCESSOR	5
2.1 Wafer-Level Description	5
2.2 Fault-Tolerance Input	7
2.3 Piecewise Linear Calibration	7
2.4 Time Alignment	10
2.5 Gamma Circumvention and TDI Summation	11
2.6 Matched Filter and Detector	14
3. IMPLEMENTATION ISSUES	19
3.1 Area Estimates	19
3.2 Serial versus Parallel Arithmetic	19
3.3 Predicted versus Actual Area	23

4. RELIABILITY ESTIMATES	25
4.1 MIL-HDBK-217E	25
4.2 Processor Element Reliability Estimate	26
4.3 FPP Reliability Estimate	26
4.4 Influence of Pairwise Interactions	27
5. CONCLUSION	31
APPENDIX A - MAXIMUM LIKELIHOOD APPROACH TO GAMMA CIRCUMVENTION	33
A.1 Maximum Likelihood Model	33
A.2 Illustrative Example and Comparison with SATDI	34
APPENDIX B - ROUND OFF IN TDI SUMMATION	39
REFERENCES	42

LIST OF ILLUSTRATIONS

Figure No.		Page
2-1	Downsized scanning array	6
2-2	Schematic wafer layout	8
2-3	Input and calibration cell	9
2-4	Time delay cell	11
2-5	Gamma circumvention and TDI summation cell	13
2-6	Matched filter and detection cell	16
2-7	FIR filters	17
3-1	Schematic area allocation on PFPP wafer – bit parallel	21
3-2	Schematic area allocation on PFPP wafer – bit serial	22
4-1	Processor reliability	28
4-2	Processor reliability with nearest-neighbor interaction	29
4-3	Effects of PE reliability	30
A-1	Probability density function	35
A-2	Log likelihood ratio	35
A-3	Receiver operating characteristic	37
B-1	Detail of proposed TDI summation circuit	39
B-2	Low background, (a) high gamma and (b) low gamma simulation.	40
B-3	High background, high gamma simulation.	41

LIST OF TABLES

Table No.		Page
3-1	Component area estimates	19
3-2	Area allocation for a PE - bit parallel	21
3-3	Area allocation for a PE - bit serial	22
3-4	Estimated versus actual cell area	23

ACKNOWLEDGEMENTS

The author, who was completely ignorant of wafer-scale technology when this work began, benefited greatly from discussions with the members of Group 23, who are doing the design and fabrication of the wafer described in this work as well as previous monolithic restructurable VLSI wafers. The contributions of A. H. Anderson, C. E. Woodward, and K. H. Konkle deserve particular mention.

A great debt is owed to Steve Pohlig of Group 27, who did much of the early conceptual design work on large-scale FPPs before the present author came to Lincoln.

Finally, it is a pleasure to acknowledge the many conversations with A. E. Filip, who shepherded the project from its inception.

DESIGN OF A WAFER-SCALE FOCAL PLANE PROCESSOR

1. INTRODUCTION

1.1 SCANNING ARRAYS

Consider a generic scanning infrared sensor, consisting of a detector array with n rows and k time delay integration (TDI) columns. (The entire arrangement may then be duplicated for each of m color bands. These will be ignored hereafter for the sake of simplicity.) One can imagine this array scanning horizontally across an image in order to form a two-dimensional picture. It moves horizontally by one column every dwell, and in addition is oversampled, typically by a factor of three, so that the entire set of detectors is read out three times per dwell. Data from a column with TDI position k must be delayed $k - 1$ of these dwells before being added to subsequent data from the same row in order to perform the time alignment needed for integration.

1.2 FOCAL PLANE PROCESSOR

The focal plane processor (FPP), also known as a time dependent processor, is responsible for the initial signal processing of data from an array of photodetectors. From a computational point of view, the initial focal plane processing is characterized by two salient points: (a) the input data stream is massively parallel: each detector in the scanning array is sampled after every dwell time and is treated essentially identically, and (b) the algorithms applied to each detector sample are relatively simple and well-understood. These two points taken together favor a hardwired, single instruction multiple data (SIMD) architecture for the FPP. This architecture, together with the requirements of low power consumption, low weight, and high reliability imposed by a space environment, makes wafer scale integration (WSI) a natural choice for the processor technology. Nonetheless, even the relatively simple processing requirements of the FPP impose a higher degree of internal differentiation on the WSI processor (i.e., more cell types) than has previously been demonstrated. Design of such a WSI processor is a nontrivial task, and represents the subject of this report.

The functions of the FPP may now be discussed in greater detail. The incoming data must be calibrated to correct for responsivity differences among detectors, and samples which have been corrupted by the effects of γ radiation need to be recognized and discarded. Following that, two other signal processing functions, time-delay integration and matched filtering and threshold detection, must be performed. At this point, the object dependent processor (ODP), whose load depends on the number of objects over threshold, takes over. These four major functional units are described briefly in the order in which the data pass through them.

1.2.1 Calibration

Each pixel in the detector array will have a slightly different dark current and responsivity, which must be corrected. If this function has not been implemented in the analog front end, it is

handled in the FPP via an addition and multiplication. In principle, nonlinear responsivities could also be calibrated out. This is rarely done in practice due to the difficulty of finding appropriate calibration standards.

1.2.2 Time Alignment

The earlier columns of the scanning array must be delayed before being added to later columns. This function, which would be performed by a CCD shift register in analog implementations, is implemented digitally as a circular buffer.

1.2.3 Gamma Circumvention

The detection of γ -affected data is very much like a CFAR detector, where the threshold is set to a certain number of standard deviations beyond the mean. A current estimate of the mean and standard deviation of the signal is obtained using various semiheuristic methods, and the ensemble of TDI samples corresponding to a given point is compared with a threshold based on this estimate. Samples above this threshold are assumed to be contaminated by γ -induced electrons and are discarded. The remaining samples are then averaged together to form the TDI output.

1.2.4 Matched Filter and Detector

The output of time alignment is then run through an FIR filter which compensates for the combined effect of oversampling and the point spread function of the optics. In the simplest implementation, the detector is simply a comparator. More sophisticated FPPs may incorporate more complicated circuitry, e.g., Laplacian filters to remove nuclear background effects.

1.3 FAULT TOLERANCE

The goal of a five-year mission lifetime, combined with the expected reliability of wafer-scale circuits, imposes a fault-tolerant structure on the design. The approach taken here is to have redundant circuit elements which may be switched in as needed via multiplexors. There is a design tradeoff to be made on the size of these fault-tolerant elements – too small, and the switching circuitry becomes cumbersome; too large, and the probability of and penalty for failure both become excessive.

As will be seen below, this tradeoff was one of the factors influencing the choice of lower-capability serial arithmetic processors, rather than higher-capability parallel ones. The fault tolerant unit was then chosen to be a complete processing element (PE), comprising all four functional units.

1.4 WAFER SCALE INTEGRATION

Design of an FPP to be realized in wafer scale technology must take into account the requirements of this technology. Chiefly, this means that it must be possible to lay out the processor on a wafer, and that the processor must be manufacturable with a reasonable yield.

1.4.1 Serial versus Parallel Arithmetic

The layout problem became evident early in the consideration of a parallel processor. Since the processor was designed for 12-bit arithmetic, utilizing a 35- μ m wire pitch resulted in each bus being 0.4 mm wide. The combination of a fault-tolerant architecture and the requirement for processing parallel TDI stages leads naturally to a design in which several buses lie side by side. The resulting "Los Angeles effect" produces a wafer in which buses are a significant fraction of the total area (see Section 3.2.) This fact led to the consideration of nibble-wide buses. One-bit nibbles were rapidly realized to be most appropriate, at least in the near term.

1.4.2 Defect Tolerance

Any process will have a small number of manufacturing defects. A circuit containing as many elements as a wafer-scale processor will have a yield approaching zero unless a way is found to correct the defects after manufacture. In the restructurable VLSI processes, redundant elements called restructurable cells are laid down. These are then connected together after testing[9]. Hence, any design must include identification of suitable restructurable cells. These cells must be relatively small (< 15,000 transistors) so that their yield is good, yet be common and few in type to simplify design and mask production. Ideally, they should bear some simple relationship to the functions of the processor. All these goals are furthered by an architecture based on a multitude of low-capability serial elements, rather than a few higher-capability parallel ones. In particular, we find that the restructurable cells can be just the four functional units discussed in Section 1.2.*

1.5 ORGANIZATION OF REPORT

This report is divided into five sections. The present section introduces an FPP and its functions to those unfamiliar with one, and to identifies the principal issues that drive the design. Section 2 begins by presenting a set of strawman requirements for a space-based IR sensor. These

* Late in the design of the wafer, the gamma circumvention circuit was in fact split into two smaller parts, one for TDI summation (left side of Figure 2-5) and one for gamma threshold generation (right side). The change was made for producibility reasons; the full gamma cell would otherwise have been 40 percent larger than the next largest cell in the PFPP. For the purposes of this report, however, the two cells will be considered as one.

requirements motivate the design of the major functional units of a prototype wafer-scale FPP, which are described in some detail in the remainder of the section.

Sections 3 and 4 give a closer look at some of the critical design methodology. Section 3 describes in more detail the area calculations which illuminated the principal problem in the initial design of the WSI prototype FPP: getting enough processors on the wafer to ensure a reasonable probability of success. Success in this sense must embrace both initial yield (defect tolerance) and reliability in use (fault tolerance). The solution to this problem is the use of bit-serial arithmetic. Section 4 describes the part-stress-analysis approach [4] used to estimate the reliability of the PFPP and its subunits. Section 4 also presents a bottom-up calculation and rationale for the reliability parameters chosen. A redundant (M-of-N) processing element architecture is employed to achieve acceptable mission life given the expected subunit reliability.

Following the report conclusion, two appendices present more in-depth treatments of roundoff errors in TDI summing, and an alternate approach to infrared detection in the presence of gamma radiation.

2. DESIGN OF A PROTOTYPE FOCAL PLANE PROCESSOR

2.1 WAFER-LEVEL DESCRIPTION

The parameters for this design were based on the conclusions of a number of classified studies reflecting the projected requirements of the Space Surveillance and Tracking System (SSTS). The strawman sensor point design calls for a sensor of 20,000 rows and 5 TDI columns in each of 4 color bands. The detector array moves horizontally by 1 column every $28 \mu\text{s}$ and is oversampled by a factor of 4 in time, so that the entire set of detectors is read out every $7 \mu\text{s}$. The dwell time used in the TDI process is $28 \mu\text{s}$.* A wafer scale (or any other) processor is unrealizable for this data rate ($4 \cdot 10^5 \text{ detectors} \times 1.4 \cdot 10^5 \text{ Hz} = 5.6 \cdot 10^{10} \text{ samples/s}$) in current technology, although one will eventually be feasible using one micron or smaller geometry and large wafers.

Instead, a prototype FPP (PFPP) was designed around a downsized scanning infrared sensor, shown in Figure 2-1. This sensor consists of a monochrome detector array with only 64 rows. However, the number of TDI columns and readout rate was retained from the strawman sensor, so that the PFPP maintains the essential design parameters of the complete sensor, but with 1250 times fewer processing elements. These PEs could then be proliferated on 6-inch wafers with $1\text{-}\mu\text{m}$ geometry, but need not be redesigned to accommodate the full strawman sensor point design.

The following list is a summary of the PFPP design, based on the above sensor description and assuming 3-inch SOI wafers with $3\text{-}\mu\text{m}$ design rules.

- (1) The processing of the 64 detector rows will be performed with a system using 2 wafers, which will contain 5 processor elements (PEs) – 4 working and 1 spare.
- (2) Each processor element processes data from 8 consecutive rows of the detector array.
- (3) Input data are assumed to be 12 bits long. This wordlength permits a mean background that is two orders of magnitude greater than the target signal. Three-percent precision (5 bits) is then possible on a signal that is one percent (7 bits) of the mean [1].
- (4) Eight detector rows are processed in the $7 \mu\text{s}$ sampling time requiring $7 \mu\text{s}/8 = 875 \text{ ns}$ per detector. In order to preserve full 12-bit accuracy throughout, the

* Since the time of these SSTS studies, the space surveillance community has moved toward less aggressive sensor designs emphasizing near-to-intermediate term producibility. Typical integration times have become an order of magnitude or more longer and the number of detector elements has decreased, although the number of TDI stages have gone up somewhat. The design for this prototype processor, however, was frozen before these changes became effective. The principal effect of implementing the changes would be to make the FPP much more memory intensive, by increasing the size of calibration memories and delay buffers while reducing the number of PEs.

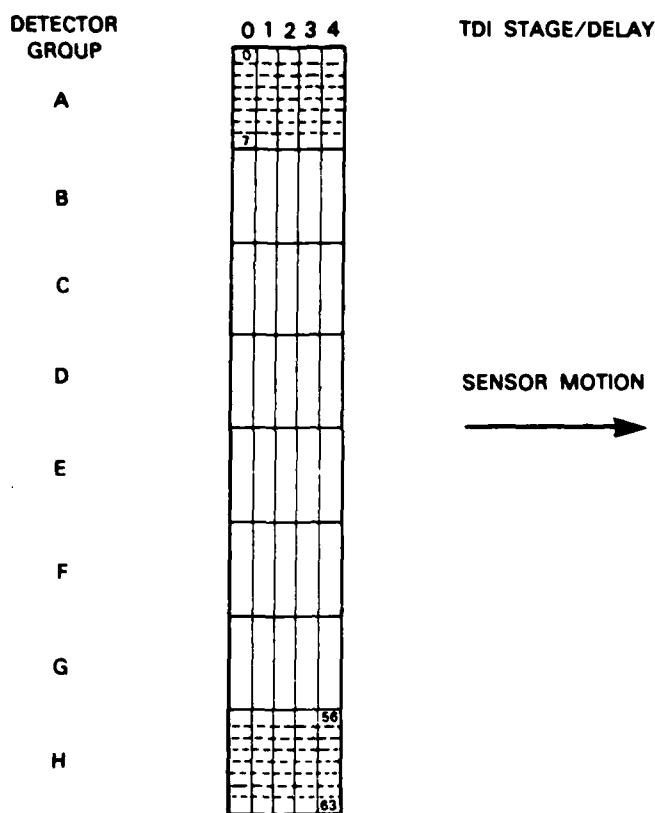


Figure 2-1. Downsized scanning array.

12-bit input data stream will be padded with 2 bits of leading zeros, providing for word growth in intermediate stages of processing. It will then be processed bit-serially. Thus, the processor clock will run at $875 \text{ ns}/14 = 62.57 \text{ ns/bit}$ (16 MHz).

- (5) Fault-tolerance is obtained by connecting the processor elements to the input and output buses through multiplexors, allowing any 2 of the 10 PEs to fail without loss of functionality.
- (6) Defect-tolerance is obtained by laying down a large number of PEs and piecing together good ones at restructuring time. Current area estimates indicate that 18 complete PEs could be laid down on a single wafer, however, fewer actually will be (see Section 3.3).

Note that only 5 of the possible 18 PEs per wafer are required to restructure the proposed system. Additional bussing and pinouts will be provided so that if yields are better than this initial conservative design goal requires, the wafer can be configured to handle a larger number of inputs.

The design still calls for a 2-wafer set in order to exercise the multiple wafer design concept which will eventually be required.

Figure 2-2 represents a quasi-geographical schematic layout of one wafer from a two-wafer processor set, with the lowest level of detail being four units - input mux/calibration/time alignment; gamma circumvention/TDI summation; matched filter/detector; and output mux. The fault-tolerant data busing is shown in detail on this figure, although the rest of the busing (e.g., off-wafer calibration, control logic, etc.) is not. This is to make the sparing strategy explicit, as well as show some of the complexity of the interconnect. Note that since the architecture is serial, all buses are only one bit wide.

2.2 FAULT-TOLERANCE INPUT

Figure 2-3 shows the input and calibration cell. Each input subunit is connected by a 4:1 multiplexor to any of 3 consecutive input signals (except for PEs on the ends of the chain) or a test pattern input. This arrangement permits any 2 PEs to fail at runtime, and to be replaced by their neighbors. Referring back to Figure 2-2, the 4 initially active PEs on the wafer are shown labeled A-D, corresponding to the array segments to which they are assigned. The second wafer (not shown), will have an identical set labeled E-H. The input subunits are also subscripted with the TDI stage to which they belong. Two spare PEs are provided, one at each end of the processor element chain, labeled X (shown in Figure 2-2) and Y (on the other wafer).

Figure 2-2 also shows output muxes for the PEs. This feature would make the sparing strategy transparent off-wafer; each output pin would always contain signals from the same input pixels. In the interest of simplicity, however, the output mux will not be implemented in the PFPP. Pins for every PE are present and the ODP will have to keep track of which are active.

In this design, the fault-tolerant atom is the whole PE. This approach, which simplifies the design concept, is made possible by the use of small low-capability serial processors. A parallel processor running at a similar clock rate, e.g., serving 96 rows instead of 8, would be too large to discard lightly.

2.3 PIECEWISE LINEAR CALIBRATION

Figure 2-3 shows the calibration circuit. The input data are processed by a piecewise linear approximation to a function which corrects for nonlinearity and nonuniformity in the detectors. There is a separate set of calibration coefficients for each of the 8 detectors assigned to a single PE. Each of these calibration functions has 4 linear segments. The appropriate slope and offset for the piecewise linear function are selected by addressing the coefficient memory with a combination of the 2 MSBs of the input data to indicate which of the 4 linear segments to use, and a counter to indicate which detector is being corrected.

The slope coefficients are stored with 10-bit accuracy. This length is sufficient to maintain the input accuracy, since each coefficient is applied over $\frac{1}{4}$ full range. Since the offset is 12 bits, each

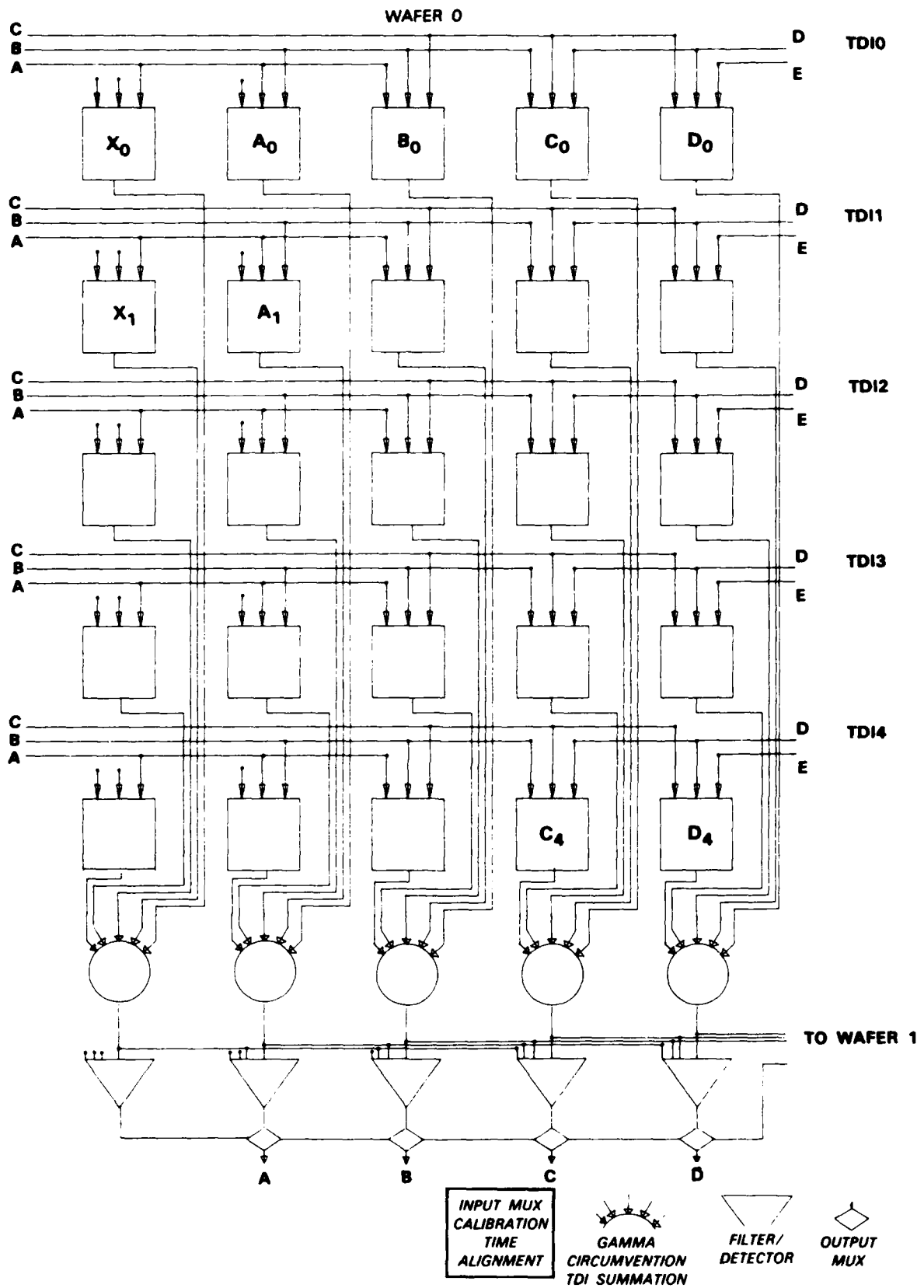


Figure 2-2. Schematic wafer layout.

calibration memory contains $8 \times 4 \times 22 = 704$ bits, which is quite modest. Memories that small tend to be dominated by their address decoding logic; an increase in integration time on the part of the focal plane would permit more rows to be handled by each PE and a concomitant increase in storage efficiency.

Although the circuit is designed to implement a 4-segment linear correction, several other functions are possible using the same circuit, but with different data in the memory, notably a simple gain and offset calibration. At present, IR systems typically use either single point (offset) or 2-point (gain and offset) calibration, due to the difficulty of finding appropriate calibration standards in the infrared. This situation is unlikely to change in the near term; the requirement of 12-bit accuracy thus translates into a rather daunting requirement on the photodiode array of linearity better than 1 part in 4096.

The SETUP logic on the right of Figure 2-3 controls the downloading of the calibration coefficients from off-wafer. Note that aside from the overflow protection, no attempt is made in the on-wafer logic to impose any reasonableness criteria on the coefficients (e.g., continuity at segment boundaries). This is the responsibility of the off-wafer calibration algorithm.

Data representation throughout the processor is positive only. This convention does not result in any loss of generality. The detector element with the highest dark current will have an offset of zero in an all positive scheme. Other elements will have pedestals added to match it. The pedestal may then be compensated out at the output threshold. Note, however, that "hotter" (higher dark current) pixels still effectively compress the available dynamic range of the processor. Allocating 1 of the 12 bits to a sign cuts the range by a factor of 2, but with a detector uniform to ± 5 percent, the largest pedestal is 410 out of 4096, giving the edge to the all-positive approach.

2.4 TIME ALIGNMENT

The time delay and integration process requires that earlier columns be delayed so that they can be processed along with later ones. In the strawman design under consideration, the unit TDI delay is $28 \mu\text{s}$. Since the last stage need not be delayed, time alignment consists of delaying each set of 32 detector inputs by 0, 28, 56, 84, or $112 \mu\text{s}$, respectively. (Recall that there are 8 detector rows per PE and each dwell is oversampled by a factor of 4.) Logically, the delay stages may be thought of as delay lines. However, implementing delay lines in CMOS is undesirable because of the large switching currents. Instead, the delays are implemented as circular buffers, in which only the address pointers are incremented while the data remain in place. A single delay stage, which is a restructurable cell in the design, is shown in Figure 2-4. Incoming data arrive in bit-serial format, are converted to parallel with a serial-in-parallel-out (SIPO) converter and are stored in a 32×12 static RAM. The read and write addresses for this memory are controlled by a counter. Since the delay is 32 words, word $n + 32$ always overwrites the location that word n was just read from. Multiple delays are implemented by daisy chaining this 32-word delay cell. The small capacity memory cell is not area-efficient by itself, but the efficiency of not constructing 4 different size memories more than compensates.

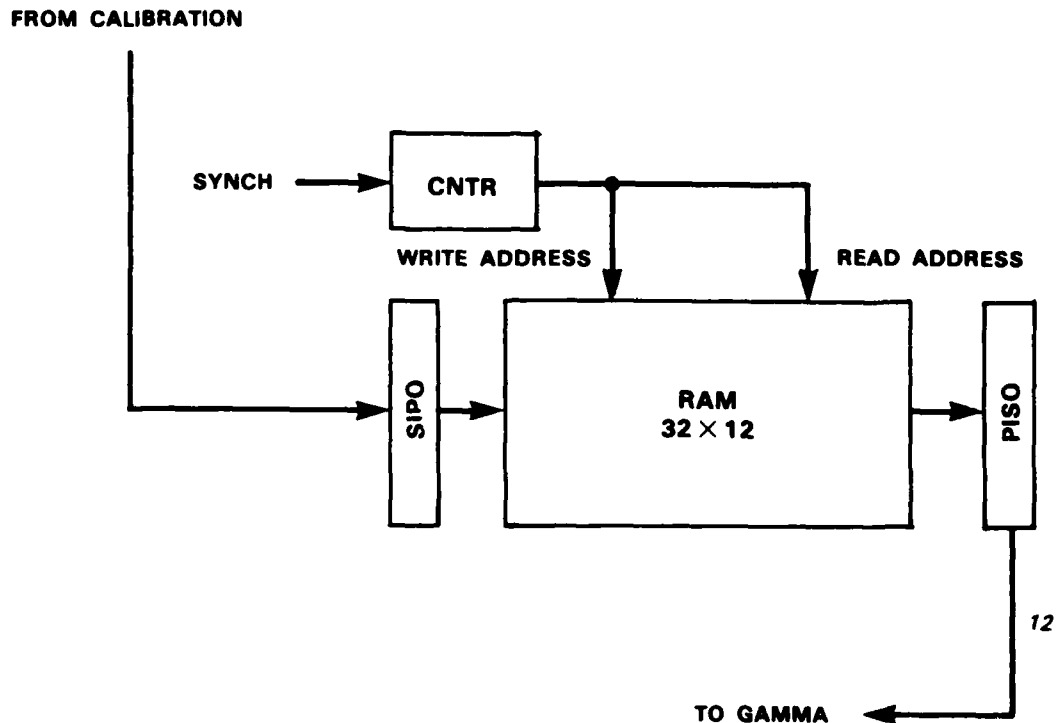


Figure 2-4. Time delay cell.

2.5 GAMMA CIRCUMVENTION AND TDI SUMMATION

The purpose of this cell is twofold: reject detector element signals which have been contaminated by γ events and then average the remaining TDI elements together. Before turning to the implementation on the PFPP, we will give a brief introduction to gamma circumvention (in order to motivate it) and an alternative approach.

What is being circumvented in gamma circumvention is noise produced not directly by γ s, but by electrons produced by the interaction of γ radiation with matter in the vicinity of the detector array. The interaction of γ radiation with matter takes place through three main mechanisms:

- (1) Photoelectric effect
- (2) Scattering on free electrons
- (3) Pair production

At the energies associated with nuclear-produced radiation, items (1) and (2) are the dominant mechanisms. (See, for example, [2] section 2-9 for a discussion of the physics.) The resultant electrons are charge carriers which produce effects in the detector similar to those produced by

IR-photon-induced carriers. They produce an energy spectrum with a long exponential falloff ("Landau tail") characteristic of the passage of ionizing radiation through matter.

2.5.1 Algorithm

The algorithm chosen is a variant of the Spike Adaptive (SATDI) type[15,16]. Many variants of SATDI exist, but all rely on the basic idea that detector response within a TDI set should be the same within some noise variation. Any sample outside some statistically determined limit is then assumed to be contaminated with a " γ " pulse, and is eliminated. A common approach (assuming unipolar spikes) is to use a lowest-of-N algorithm, in which the lowest TDI sample is considered to be the one most likely free of contamination. This algorithm is easy to implement in digital logic. Because of its theoretical attractiveness, however, the approach taken here is to model the data as a Poisson random variable with mean λ and standard deviation $\sqrt{\lambda}$. The estimated parameter $\hat{\lambda}$ is formed by summing the 5 TDI samples and scaling by $\frac{1}{5}$. The threshold is then formed as

$$\hat{\lambda} + k\sqrt{\hat{\lambda}}$$

where k is the number of standard deviations used.[†] A TDI sample which exceeds the threshold is considered contaminated and excluded.

2.5.2 Alternate Approach

The thrust of all SATDI approaches is to consider the γ -contaminated samples to be bad data, eliminate them, and proceed with processing on the remaining data. The SATDI approach has two disadvantages:

- (1) The signal-to-noise ratio is degraded, for the discarded samples no longer contribute to the \sqrt{N} SNR gain.
- (2) The output becomes biased, as the γ threshold eliminates samples with large positive random variation.

An alternate approach is to perform a maximum likelihood detection algorithm on the signal in the presence of γ noise. This approach is feasible if a parametric form of the γ noise is assumed, and is explored in more detail in Appendix A.

2.5.3 Threshold Generation

Figure 2-5 shows the schematic for the gamma circumvention and TDI summation cell. It is

[†] Note that Poisson statistics apply in this form only to the raw photodetection process. If the detector output has been scaled down by some factor s at the input stage, then the standard deviation becomes $\sqrt{s\lambda} = \sqrt{s}\sqrt{\lambda}$. Thus, the threshold factor k must effectively be rescaled by \sqrt{s} .

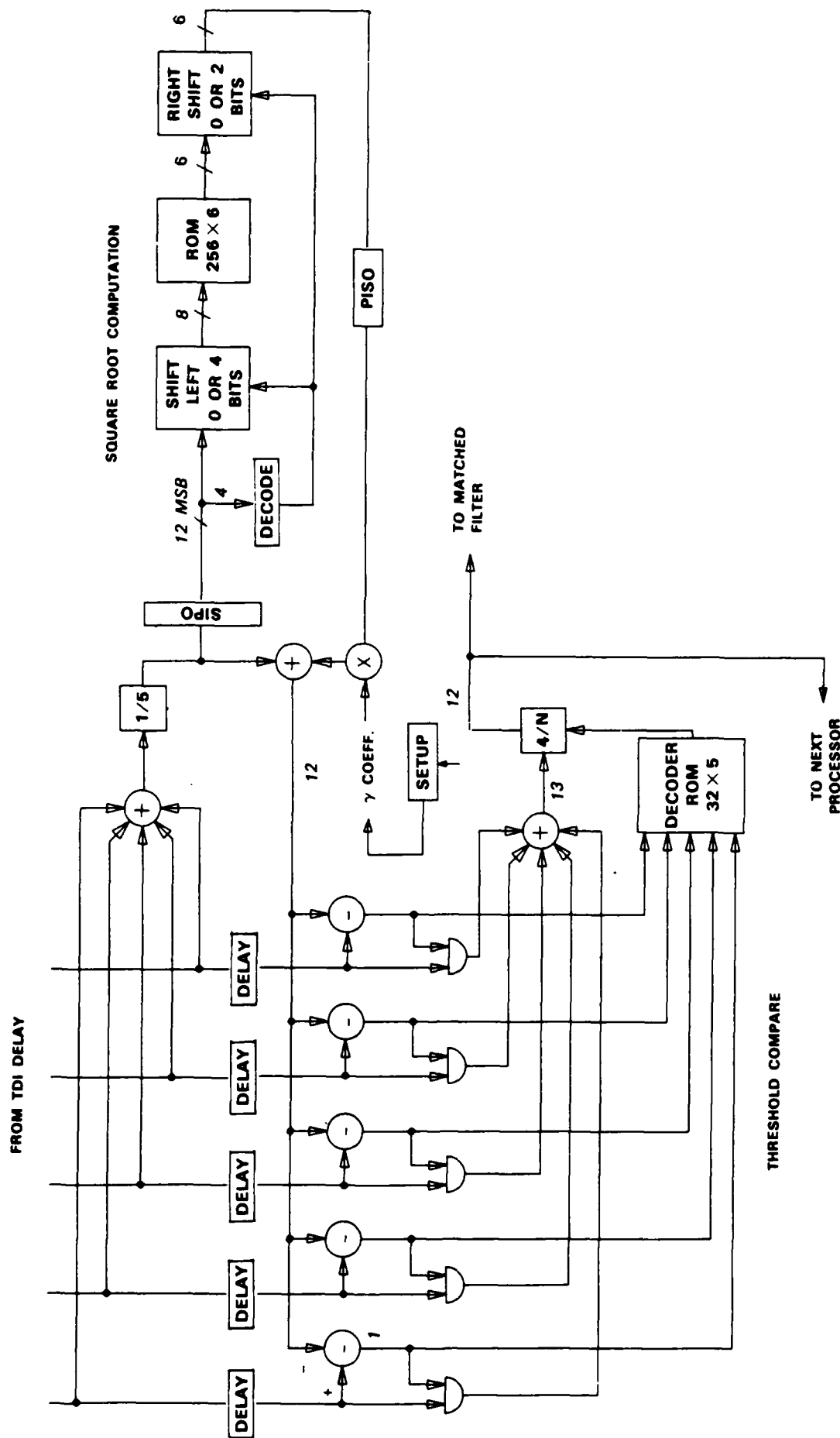


Figure 2-5. Gamma circumvention and TDI summation cell.

broken into two logical sections: the upper part generates the SATDI threshold, while the lower part compares each TDI sample with the threshold and averages the accepted samples.

Threshold generation in SATDI is a reasonably heuristic affair; consequently there is no requirement of extreme precision in the threshold generation circuit. The $\frac{1}{5}$ circuit is approximated by

- (1) Summing the 5 inputs
- (2) Rounding and shifting right 2 bits, leaving a 13 significant digit sum
- (3) Multiplying the sum by $\frac{4}{5}$, approximated to 6 bits as $0.110011_2 = 0.796875_{10}$ for a 0.4 percent error.

See Appendix B for a further discussion of this approach.

To save space, the square root is calculated using a 256×6 ROM. As shown in Figure 2-5, the method is a 2-range lookup table. The 12-bit input data are shifted left 4 bits if the data item is less than 256, and the resulting 8 MSBs are then used to address the table. This shift maps the ranges 0 to 255 and 256 to 4095 into a single 256 element table. The output of the table is compensated by shifting right 2 places if the input is shifted left. The dual-range lookup yields a maximum difference of 1 from a true integerized square root over the range 0 to 4095.

The output of the square root table, which represents an estimate of the standard error, is then multiplied by a 5-bit γ constant and the product is added back into the delayed average to form the SATDI threshold. The multiplier is arranged so that the output is scaled by $\frac{1}{8}$. Thus, the γ constant is effectively in the form $xx.xxx$, allowing a range of 0 to 3.875 in steps of 0.125.

2.5.4 Comparator and TDI Summation

The output of the SATDI generation circuit is fanned out and compared with the delayed TDI set in parallel. Those elements which are under threshold are passed through to a summer. The output of the comparator is also passed to a circuit which generates a multiplier for scaling the summer output. The multiplier is $4/N$ rather than $1/N$ because the summer has prerounded and right-shifted the sum bits by 2, in order to guarantee that the maximum number of nonzero bits is 13. Proceeding in this manner, which is advantageous from a hardware point of view, can cause an error in the least significant bit. The effect is not significant except when the signal and background are both small. Appendix B contains a more detailed discussion.

2.6 MATCHED FILTER AND DETECTOR

The matched filter is a separable 4×4 digital filter. Being separable means that the filter may be constructed as the convolution of a 4-tap filter oriented vertically with another 4-tap filter oriented horizontally, resulting in a savings in the amount of computation required. The 4-tap

horizontal filter is matched to the $4\times$ in-scan oversampling. The 4-tap vertical filter assumes that the cross-scan resolution is made comparable to the in-scan resolution by using rectangular pixels.

The matched filter and detector cell is shown in Figure 2-6. A far more detailed hardware description is given in [3]. Much of the complication of the interconnect stems from the fact that the cross-scan filter requires data from adjacent detector rows and hence adjacent PEs. The most naïve design would require data from both nearest neighbors; the current implementation offsets the cross-scan filter so that a PE only requires data from the previous PE (Figure 2-7). The output of the PE can then be shifted up to compensate for this offset (ignoring edge effects).

The 8×12 delays are implemented as true shift registers in this design, resulting in a significant current draw. A more capable PE would require longer delays and these could also be implemented as circular buffers like the time alignment memories.

A simple threshold detector is attached to the output of the horizontal convolution. The threshold is loaded from off-wafer, so that it can be adjusted during operation of the PFPP as a means of controlling the overall false alarm rate. The comparator is implemented as a combinatorial full adder, and the full signed difference is sent off-wafer to the ODP.

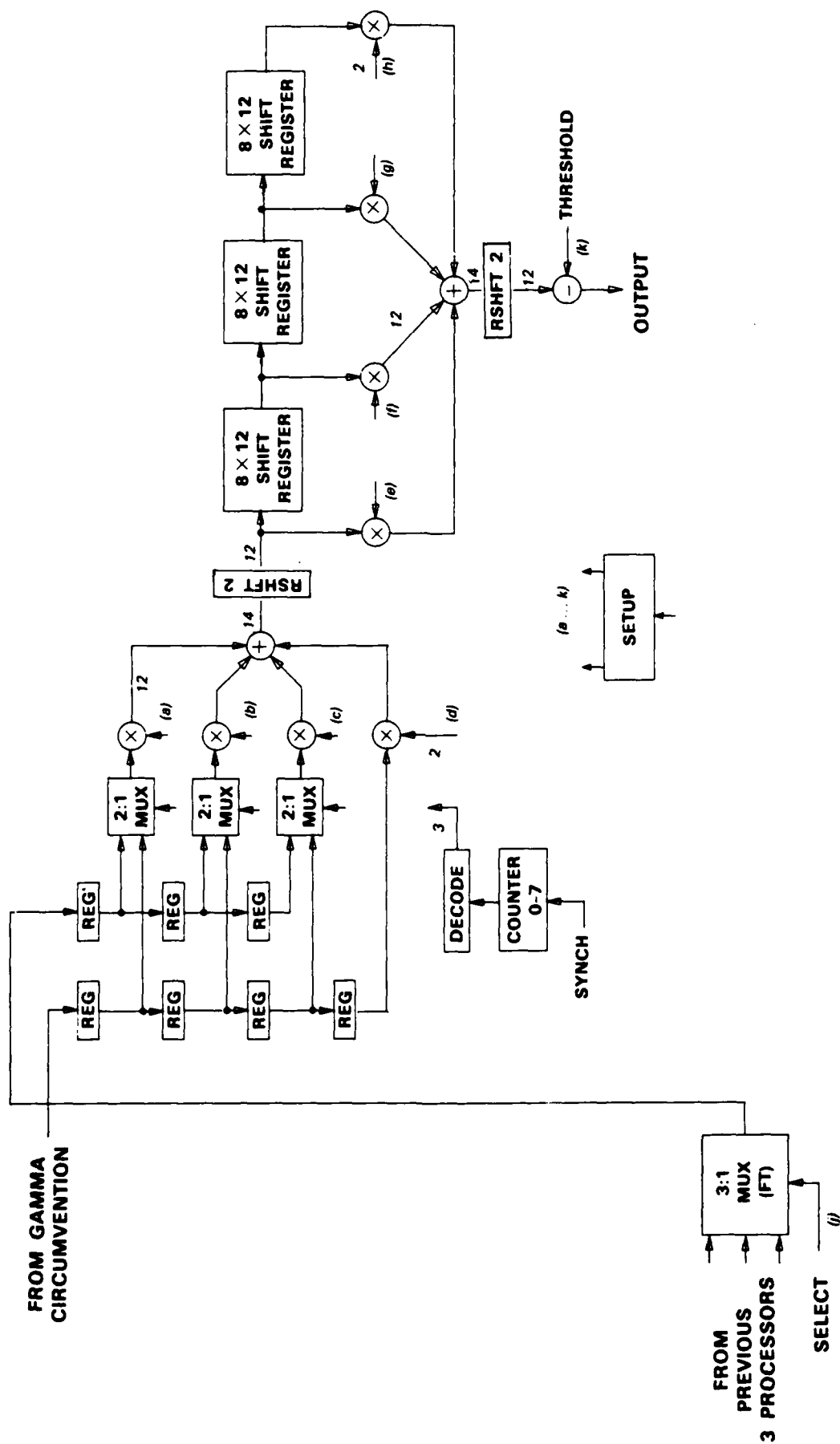


Figure 2-6. Matched filter and detection cell.

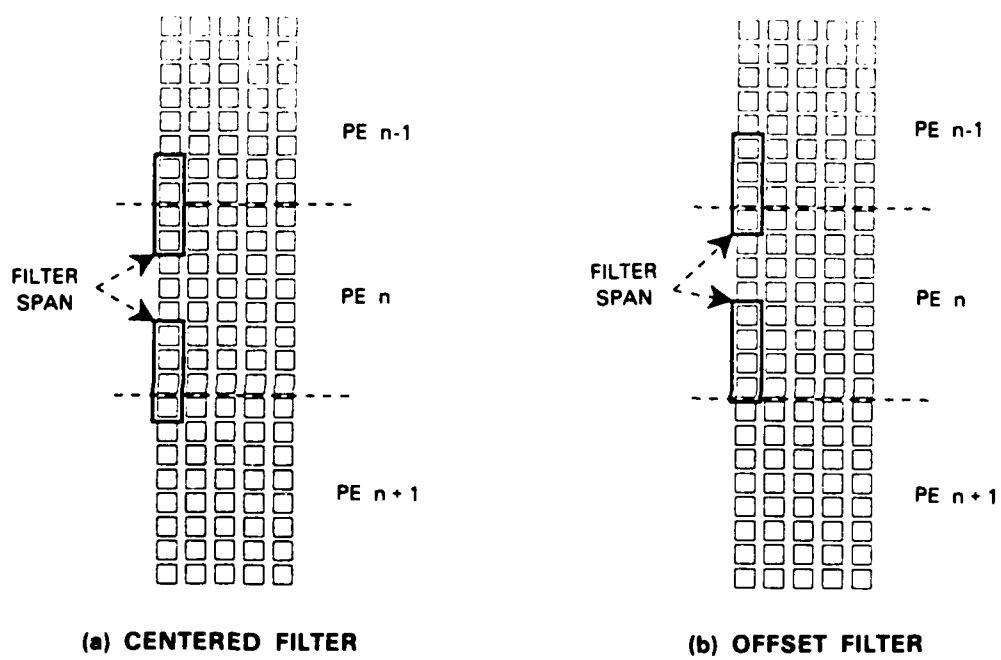


Figure 2-7. FIR filters.

3. IMPLEMENTATION ISSUES

3.1 AREA ESTIMATES

In the course of the conceptual design of the wafer, area estimates were done using relatively crude estimates of the circuit elements needed in the design. The area required for certain circuit components was estimated as shown in Table 3-1. The estimates for static RAM and shift registers

TABLE 3-1.
Component Area Estimates

Component	Area (mm ²)
Static RAM, per bit	0.0063
Shift register (static), per bit	0.0081
Serial multiplier, per bit	0.1200
Serial adder, per bit	0.0580
Tristate register, per bit	0.0225

were from designs being developed by Group 23 at Lincoln Laboratory. The memory figure assumed a cell size of $40\lambda \times 50\lambda$, and amortized the area required for read/write and address select over the per-bit figure. This area is nonnegligible for small memories as are used in this design. The remaining estimates were from MOSIS scalable designs with $\lambda = 1.5$ (for $3\text{-}\mu\text{m}$ technology).

3.2 SERIAL VERSUS PARALLEL ARITHMETIC

Using these figures, area estimates for both a serial and a parallel arithmetic processor were developed. For equal clock rates, the parallel processor will have 12 times the capability of the serial one.* One might naïvely expect each serial processor to be $\frac{1}{12}$ of an equivalent parallel processor in area (see [12], p.20). This is not the case for a number of reasons:

- (1) Extra accumulator registers have to be provided for the multipliers.
- (2) Extra shift registers have to be provided for increased latency at choke points where all bits are required (e.g., calibration, gamma circumvention).

* For ease in supplying input data, the prototype parallel processor was sized for only 16 detector rows rather than 96; it was designed to run in burst mode, with a low duty cycle.

- (3) Calibration and TDI delay memories become less dense as their size is reduced to serve fewer detectors.
- (4) Since serial adders are pipelined, intermediate word growth that appears when summation is followed by division, e.g., TDI summation, has to be accommodated by padding out the bit stream with extra zeros.

Figures 3-1 and 3-2 are graphical representations of the area estimates for the PFPP using parallel and serial arithmetic. Inset into them, in turn, are Tables 3-2 and 3-3 which present the data numerically and serve as the figure keys. In the figures, space allocated to a PE is represented by the horizontal chaindash bars. Within the bars, shaded boxes represent area allocated to circuit elements; white space around the boxes is reserved for interconnect. The crosshatched areas at the left and right are input and output buses.

The figures graphically illustrate the smaller granularity of the bit-serial architecture. Due to the significantly larger size of a parallel-arithmetic PE, and the width of the buses, only 6 (optimistically) would fit on a 3-inch wafer. The sparing strategy was to have 3 working PEs (2 active and 1 spare) per wafer. Eighteen serial processors were calculated to fit in the 50-mm square contained within a 3-inch wafer. Since only 5 are needed in the prototype system, this approach would permit a working processor even if early yields in the SOI process were relatively low.

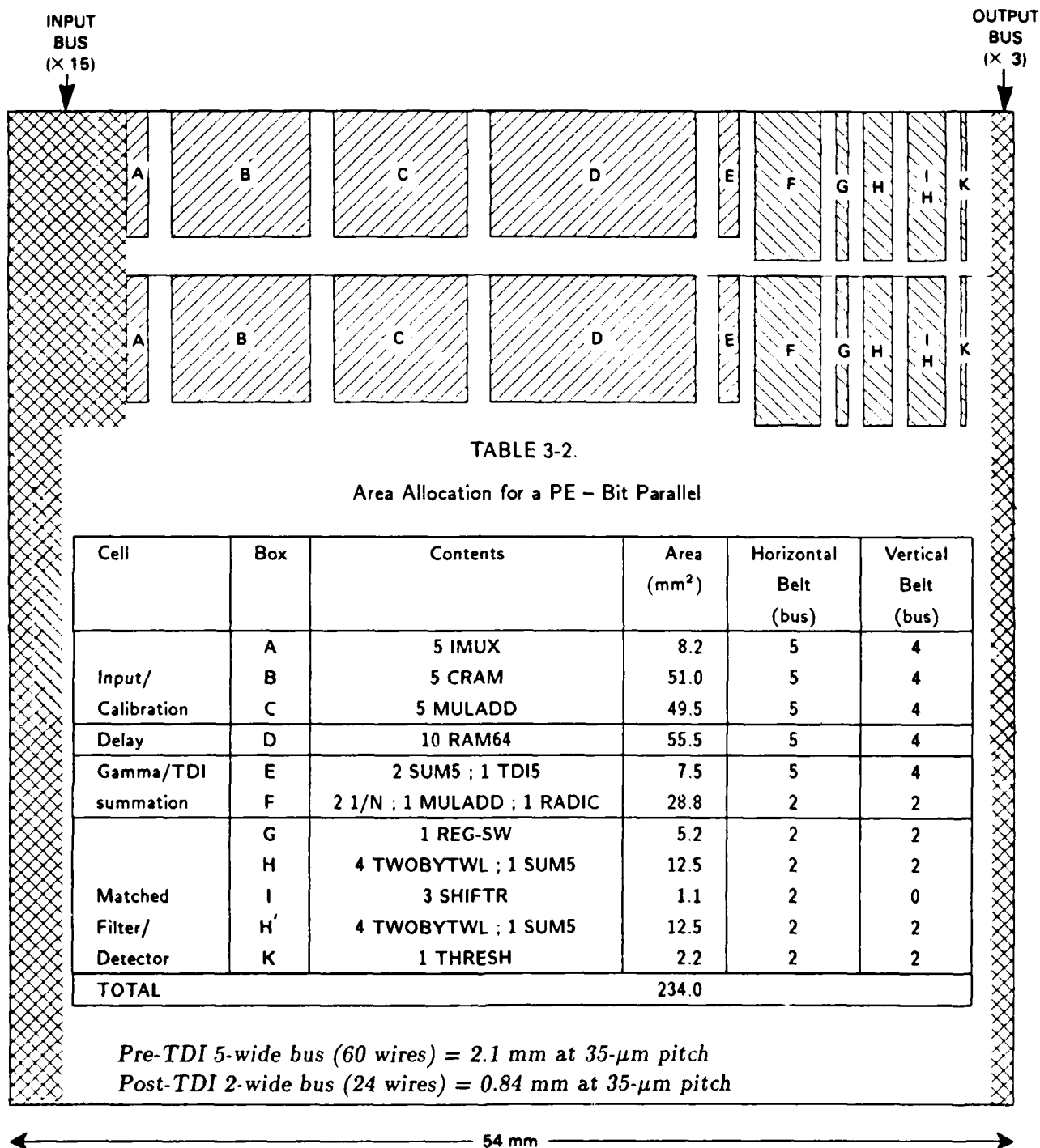
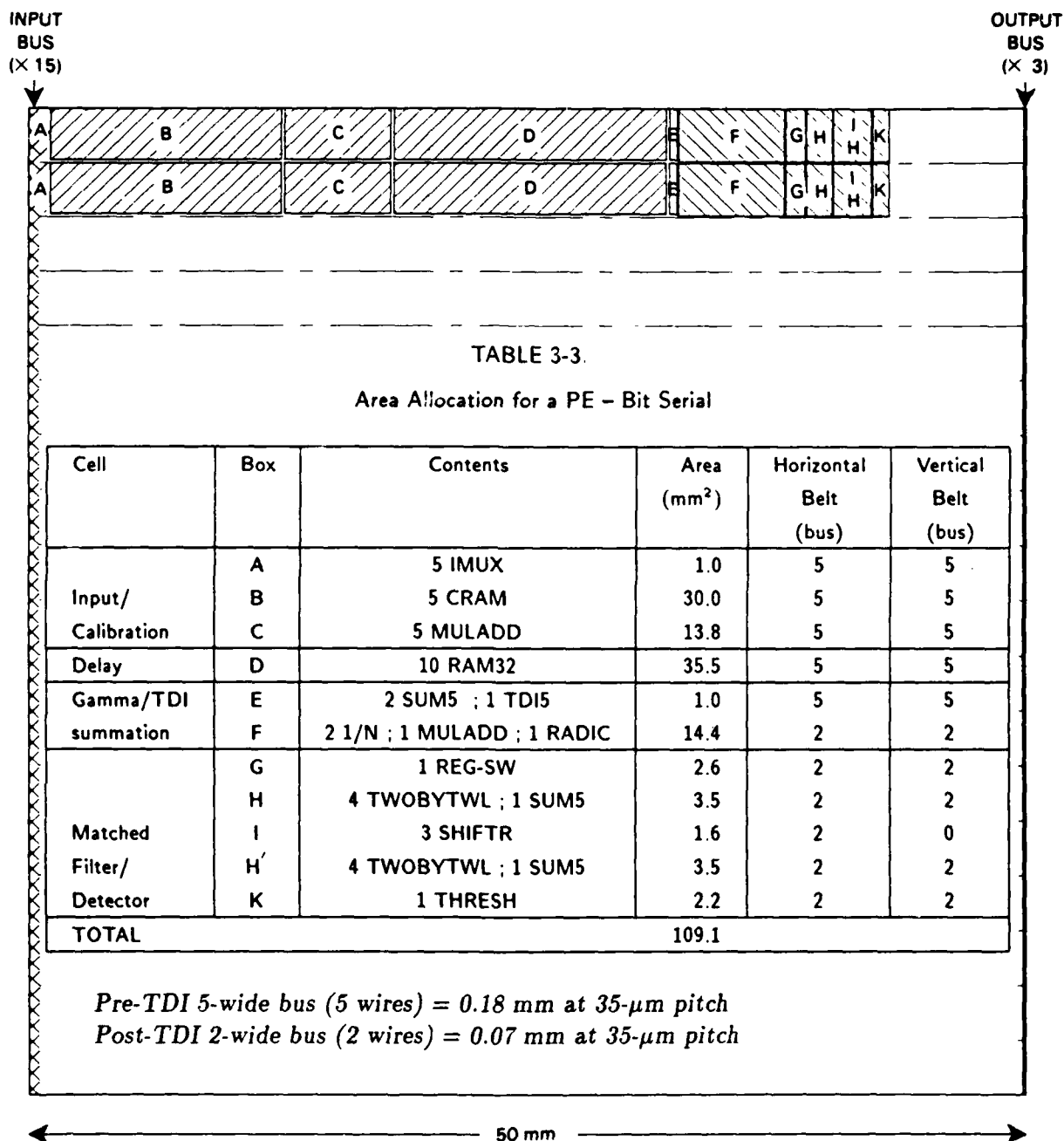


Figure 3-1. Schematic area allocation on PFPP wafer - bit parallel.



103551-9

Figure 3-2. Schematic area allocation on PFPP wafer - bit serial.

3.3 PREDICTED VERSUS ACTUAL AREA

Another interesting comparison can be made between the estimates given in Table 3-3, which were generated roughly a year before the present report was written, and the actual area taken by the cells. As of this writing, two of the four cells (TDI delay and matched filter/detector) have been designed by Group 23 and received back from MOSIS. A third (input and calibration) is in final layout and its size can be estimated with confidence. The fourth (gamma circumvention/TDI summation) is well along, and its area can be estimated with reasonable accuracy. This comparison is made in Table 3-4.

TABLE 3-4.
Estimated versus Actual Cell Area

Cell	Estimated (mm ²)	Actual (mm ²)	Difference (%)
Input/calibration	9.0	≈10	≈11
TDI delay	3.5	3.4	-3
Gamma/TDI summation	15.4	≈17.5	≈14
Matched filter/detector	13.4	10.0	-25

Agreement between the rough calculations and as laid-out areas is remarkably good. At the time of the initial calculation (16 June 1987), Group 23 had a reasonable idea of what its small static RAM would look like; hence the input/calibration and delay estimates are much closer than the other two cells. Early memory estimates, based on large commercial RAMS, had tended to be much more optimistic. Since the errors on gamma/TDI summation and matched filter/detector roughly cancel, it is reasonably certain that the goal of laying down 18 PEs on a 50-mm square could be met.

Early results with wafer scale circuits implemented in the Lincoln Laboratory zone melt refined (ZMR) SOI technology (see [10] for a review), however, indicate that defects in ZMR wafers tend to occur preferentially at the edge of the wafer. Therefore, the preliminary FPP is being designed to fit into a 40-mm square, allowing a 5-mm buffer on all edges: $(\frac{40}{50})^2 \times 18 = 11.5$; because of inefficiencies in packing, probably about 10 PEs will fit in this smaller area.

4. RELIABILITY ESTIMATES

One of the most stressing demands on a focal plane processor is the requirement of reliability in a space environment. The FPP is designed for a nominal five-year lifetime. Modern integrated circuit design results in highly reliable circuits. The extremely large number of circuit elements, however ($\approx 12,000$ transistors in the matched filter/detector cell alone), results in a rather small total probability for a system working perfectly for five years.

It is vital to design reliability in from the beginning in order to have any realistic hope of achieving mission requirements. On the other hand, precise reliability measurements are obviously lacking in any new design, and more so than usual in rad-hard wafer-scale technology. As discussed previously, the approach taken for the PFPP is to utilize a redundant network of processor elements. In order to evaluate this approach quantitatively, the reliability of an individual PE must be estimated; if the PE is too complex, the survival rate will be too small. In this case, sparing must be provided at a lower level, or a large number of spare PEs must be allocated. Thus, some sort of estimate of PE reliability must be found in spite of the novelty of the technology. A certain amount of sloppiness in the estimates must be tolerated, and the sensitivity of the overall PFPP reliability to this uncertainty must be at least estimated.

4.1 MIL-HDBK-217E

Recognizing the problem, DoD has issued MIL-HDBK-217E, *Reliability Prediction of Electronic Equipment* [4]. This handbook presents failure models of electronic components and systems, as well as constants for evaluating the models based on experience to date.

Section 5.1.2 of [4] presents a failure rate prediction model for monolithic microelectronic devices. This model is:

$$\lambda_P = \pi_Q \cdot (C_1 \pi_T \pi_V + C_2 \pi_E) \cdot \pi_L$$

where

λ_P	is	the predicted device failure rate in failures/ 10^6 hours,
π_Q	is	the quality factor,
C_1	is	a circuit complexity factor, depending on transistor count and technology,
π_T	is	the temperature acceleration factor,
π_V	is	the voltage stress derating factor,
C_2	is	a package complexity factor,
π_E	is	the application environment factor, and
π_L	is	the device learning factor.

For the purposes of our discussion, let us consider this as

$$\lambda_P = \pi_Q \pi_L \cdot \underbrace{(C_1 \pi_T \pi_V)}_{\text{Term 1}} + \underbrace{C_2 \pi_E}_{\text{Term 2}} \quad (4.1)$$

4.2 PROCESSOR ELEMENT RELIABILITY ESTIMATE

Term 1 applies to failures of individual PEs, and hence will be reduced by PE sparing; Term 2 applies to packaging failures. Since the pinouts are not redundant in the current design, Term 2 will not be affected by our sparing strategy – failure of a pin will reduce the capability of the wafer to perform its mission. Clearly there is not a lot of field experience with wafer-scale SOI. However, in order to proceed with quantitative analysis of a PE, we must evaluate the various factors of Term 1 as best we can. (Note that references to Table 5.1.... in this and Section 4.3 are to tables in [4], *not* this report.)

C_1 : As might be expected, MIL-HDBK-217 has no data directly applicable to wafer-scale devices. Hence, values for C_1 must be extrapolated from data it presents. Of the devices that might be applicable to the FPP case, Section 5.2.1 presents data for shift registers, static RAMs, and microprocessors in CMOS. The approach taken here is to simply calculate the C_1 for each, and then sum them. (Adding probabilities of failure is equivalent to multiplying probabilities of success as long as $P_F \ll 1$) We have

Device	C_1
Shift register (<1000 gates)	0.02
Static RAM (<16 K)	0.10
Microprocessor (16 bit)	0.06
Total	0.18

π_T : This factor depends on the technology and the worst-case junction temperature. For the *space flight* environment, worst-case case temperature is specified as 45 °C. The rise over case temperature is difficult to estimate with any precision; the PFPP wafer may dissipate ≈ 5 W (the Lincoln Laboratory fast Fourier transform wafer dissipates ≈ 3 W at 16 MHz)[6]. This heat will not be produced uniformly over the surface of the wafer, however. A wild guess for the worst-case junction temperature rise is $T_J = 15$ °C over the case temperature, or 60 °C. This choice yields $\pi_T = 0.95$ from Table 5.1.2.7-8.

π_V : This is 1.0 from Table 5.1.2.7-14.

4.3 FPP RELIABILITY ESTIMATE

To complete the analysis of the wafer, we will first evaluate Term 2 of equation 4.1 to gain an estimate of wafer reliability without sparing; then we will add in the sparing combinatorics.

C_2 : The package complexity factor is given in Table 5.1.2.7-16 as

$$C_2 = 3.0 \times 10^{-5} N_P^{1.82}$$

for hermetic flatpacks. This equation is only valid up to $N_P = 24$ pins. However, blithely extrapolating to 40 pins for the prototype FPP, we obtain $C_2 = 0.188$. Note that for a 6-inch wafer of ≈ 500 pins, this equation yields $C_2 = 2.5$, suggesting that redundant pinouts (or much improved packaging) will be an important part of the design strategy for the full-up FPP.

π_E : The space flight environment S_F is relatively benign, and from Table 5.1.2.7-3 $\pi_E = 0.9$.

π_L : The learning factor π_L is taken to be 10 in the case of a new device in initial production and/or a new and unproven technology.

π_Q : The quality factor π_Q is keyed to the military classification system established in MIL-STD-883. It is given as

Class	π_Q
S	0.25
S-1	0.75
B	1.0

Since the FPP would clearly not be listed on QPL-38510, I have considered it to be Class S-1, and assigned $\pi_Q = 0.75$.

For small numbers of PEs, there are roughly 8 pins per PE (5 TDI inputs, 1 output, 1 prior PE reference, and 1 control). Rewriting equation 4.1 in terms of N_{PE} , the number of PEs, and evaluating constants, we obtain for a wafer without sparing

$$\lambda_P = 7.5 \cdot \underbrace{[0.17N_{PE}]}_{\text{Term 1}} + \underbrace{2.7 \times 10^{-5}(8N_{PE})^{1.82}}_{\text{Term 2}} \quad (4.2)$$

For $N_{PE} = 8$, Equation 4.2 evaluates to Term 1 = 1.36 and Term 2 = 0.05, confirming our intuition that (for relatively simple packaging) PE sparing is most important. Wafer reliability over 5 years is evaluated using Equation 4.2 in Figure 4-1(a) for various numbers of PEs on a single wafer without sparing. As can be seen, although the probability of survival for a single PE $P_0 = 0.946$, for the 8 PEs required to do the job, predicted reliability $P_0^8 = 0.64$, which is rather poor.

Figure 4-1(b) shows the effect of sparing for a 2-wafer set. System reliability rises dramatically as the first 2 spares are introduced, then levels off and begins to fall slightly, so that additional spares are not helpful. This effect is due to Term 2, the projected packaging failure rate, since the PE sparing term alone continues to rise to 1. Hence, redundant pinouts will have to be introduced to raise system reliability above the ~ 97 percent level in this failure model.

4.4 INFLUENCE OF PAIRWISE INTERACTIONS

A further question which arises in the context of FPP reliability calculations is the effect of correlated failures. Section 4.3 assumes that the individual PE failure rates computed according to MIL-HDBK-217E are statistically independent, and combines them accordingly.

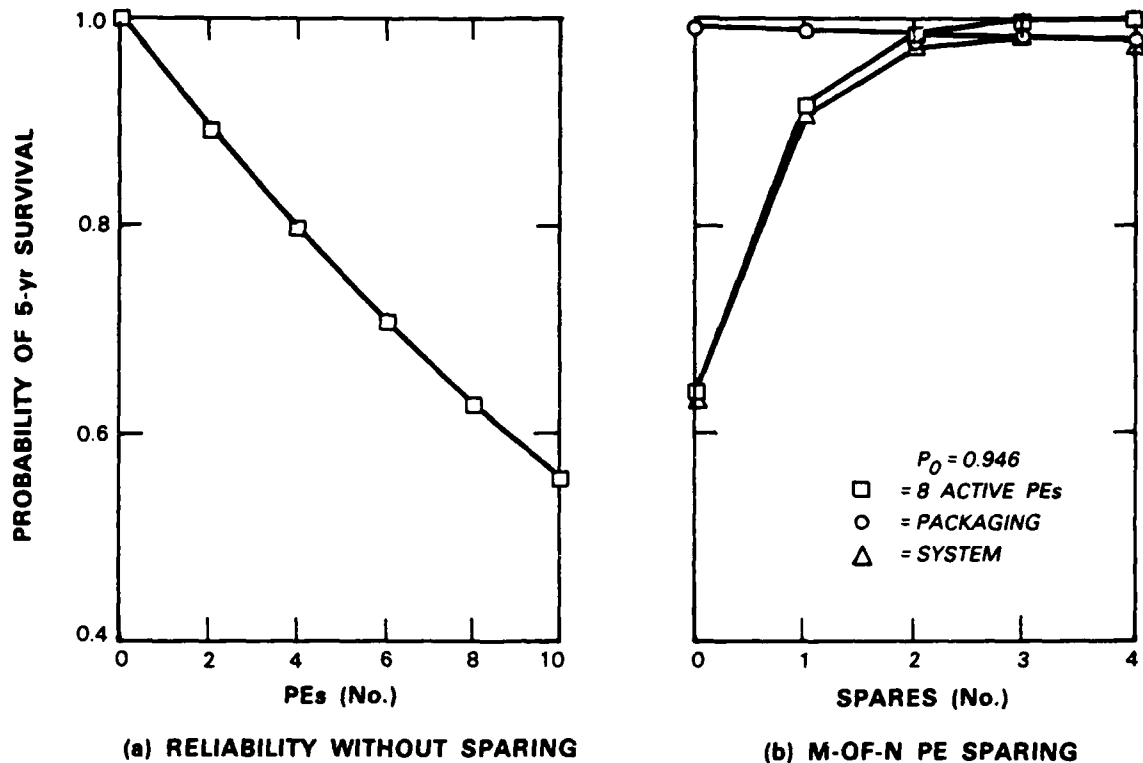


Figure 4-1. Processor reliability.

However, it is possible that the failure of one PE might somehow stress its neighbors (e.g., by dragging down bus voltage). In this case, failure of one PE would increase the probability that its neighbors would fail, so that $P_{fail}[PE_i|PE_{i\pm 1}] > P_{fail}[PE_i]$.

The approach taken here is to assume that the failure probability calculated from MIL-HDBK-217E is that of an isolated processor; nearest-neighbor interaction is then added by multiplying by a tri-diagonal interaction matrix containing the nearest-neighbor interaction C_{NN} (This approach assumes $P_{fail} \ll 1$):

$$\begin{bmatrix} P_{fail_1} \\ \vdots \\ P_{fail_8} \end{bmatrix} = [P_{fail_1} \cdots P_{fail_8}] \begin{bmatrix} 1 & C_{NN} & 0 & 0 & \cdots \\ C_{NN} & 1 & C_{NN} & 0 & \cdots \\ 0 & C_{NN} & 1 & C_{NN} & \cdots \\ & & & \ddots & \\ \cdots & 0 & C_{NN} & 1 \end{bmatrix}.$$

Not all P_{fail_i} are the same using this approach, and the sparing calculation is modified to incorporate this fact.

Figure 4-2 presents the results of the a calculation of the 5-year probability of success for various C_{NN} as a function of the number of spares, using the PE failure rate calculated from MIL-HDBK-217E. For $C_{NN} = 0.2$, 2 spares are adequate to keep the overall probability of success above 0.95.

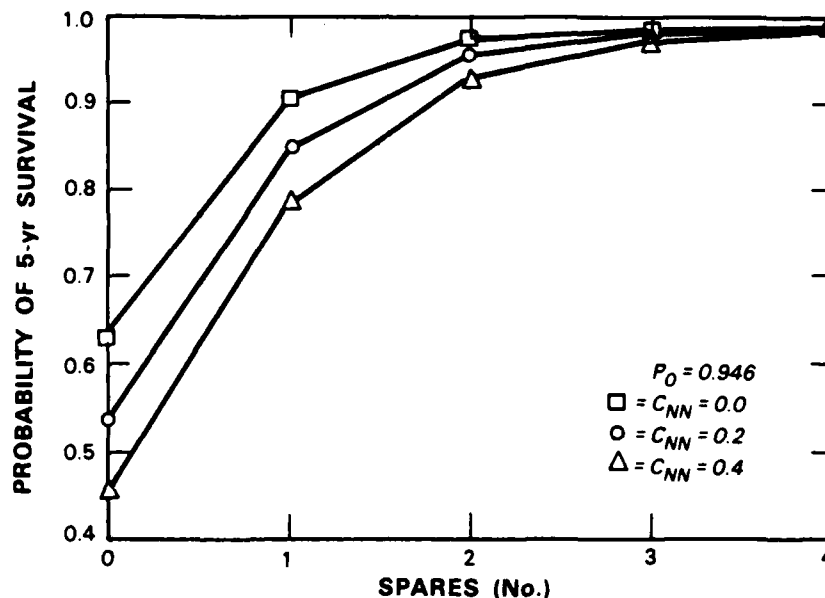


Figure 4-2. Processor reliability with nearest-neighbor interaction.

Since the rate calculations from [4] are far from exact, it is worthwhile looking at what sort of margins the sparing strategy provides. Thus, we conclude this discussion by examining the reliability of the 8-processor PFPP system as a function of the probability of survival of the individual PEs. Figure 4-3 shows the overall probability of survival as a function of a single PE's probability of survival, for the case of $C_{NN} = 0$ and $C_{NN} = 0.2$. For the no-interaction case with 2 spares, the system probability of 5-year survival stays above 0.9 as long as the single-PE probability is also above 0.9. With $C_{NN} = 0.2$, this threshold is increased to ~ 0.925 . Increasing the number of spares to 4 gives a system probability of survival > 0.9 as long as an individual PEs probability of survival is > 0.8 for the no-interaction case.

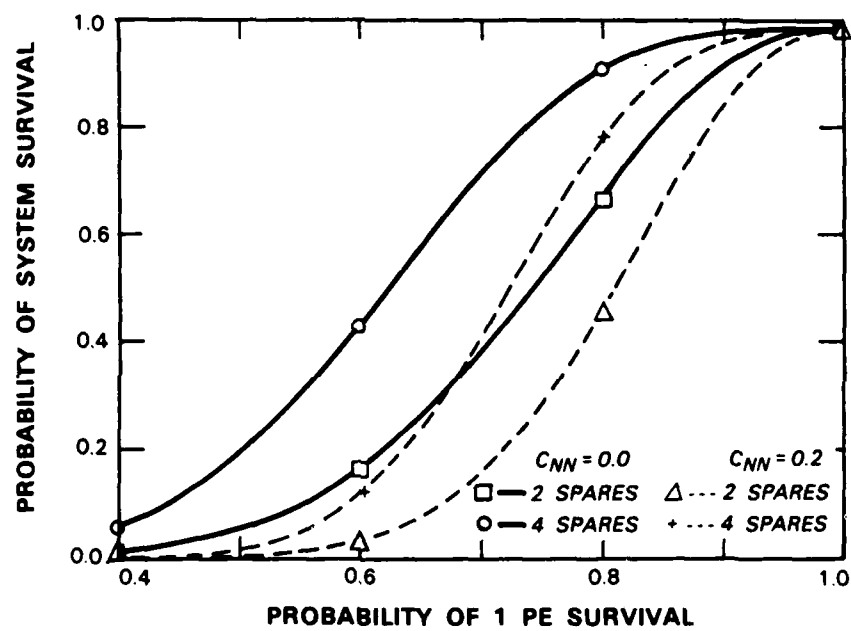


Figure 4-3. Effects of PE reliability.

5. CONCLUSION

We have described the design of a prototype wafer-scale focal plane processor. This design represents an evolution from previous work in monolithic VLSI, as it has four different cells in each PE, rather than a relatively uniform array of cells as in earlier work[7,8]. The design incorporates fault-tolerant technology in order to achieve a five-year lifetime with predicted 97 percent confidence.

Wafer-scale technology represents an important advance in focal plane processors for space-based applications. Current processors in aircraft-based applications, with only medium levels of integration, occupy several cubic feet of volume and dissipate several thousand watts[5]. By comparison, a processor based on wafer-scale technology would be at least an order of magnitude smaller in both parameters.

APPENDIX A

MAXIMUM LIKELIHOOD APPROACH TO GAMMA CIRCUMVENTION

Since the early 1970's, there has been a great deal of effort expended on increasing the immunity of infrared sensor systems to the effects of γ radiation. The most successful approach by far has been to harden the focal plane. Developments in detector technology have resulted in an enormous decrease in detector volume, which has reduced the detector cross section by several orders of magnitude. The consensus is that the easy gains have been made, so that absent any breakthroughs such as intrinsic event discrimination, the next order-of-magnitude increase will be a lot harder than the previous four.

At the same time, electronic γ circumvention has made great strides. Given the difficulty of pushing the state of the art in detectors and the computational resources expended on circumvention, it is worthwhile to reexamine the field.

The most successful approach to γ circumvention to date is a two-stage algorithm, the spike adaptive time delay and integration (SATDI) method pioneered by Boeing. This heuristic approach makes no assumptions about γ -induced noise except that it is an additive corruption of the true signal (assuming unipolar γ spikes, as we will do throughout). The first stage of the method utilizes all the TDI signals corresponding to a given point in space to set an upper bound on a reasonable signal. Signals above this bound are assumed to be corrupted by γ spikes, and are discarded. In the second stage, detection proceeds normally on the cleaned-up sample.

A.1 MAXIMUM LIKELIHOOD MODEL

If, however, one is willing to make assumptions about the form of the γ -induced noise distribution, it is possible to design an optimal detector for a given signal in the presence of this noise utilizing classical maximum likelihood detection theory. The rest of this appendix reports on such a detector, utilizing the formalism developed in H. L. Van Trees[14], Chapter 2.

The parametric form chosen is an exponential distribution, $\lambda e^{-\lambda r}$ where r is the received signal, which is a reasonable approximation to the observed γ spectrum in IBC detectors.[13] The noise model is thus the sum of (a) Gaussian background noise with variance σ^2 and mean μ , (b) exponential γ noise with mean $1/\lambda$ and a probability of occurrence in a given sample f . That is, if n_T is the total noise,

$$n_T = n_B + n_\gamma \quad (\text{A.1})$$

$$p_{n_B}(n_B) = N(\mu, \sigma) \quad (\text{A.2})$$

$$p_{n_\gamma}(n_\gamma) = f\lambda e^{-\lambda r} + (1-f)\delta(0) \quad (\text{ignore multiple hits}) \quad (\text{A.3})$$

Adding random variables is equivalent to convolving their pdf's, so (adopting the notation of Van Trees) the probability density under the null hypothesis is

$$p_{r_i|H_0} = f\lambda Q(-\alpha/\sigma) \exp\left[\frac{\lambda}{2}(\sigma^2\lambda + 2\mu - 2r)\right] + \frac{(1-f)}{\sqrt{2\pi}\sigma} e^{-(r-\mu)^2/2\sigma^2} \quad (\text{A.4})$$

$$= \mathcal{F}(r_i; \mu, \sigma, \lambda, f) \quad (\text{A.5})$$

where

$$\alpha = r - \mu - \sigma^2 \lambda \quad (\text{A.6})$$

$$Q(x) \equiv \frac{1}{\sqrt{2\pi}} \int_x^\infty e^{-t^2/2} dt \quad (\text{A.7})$$

We let hypothesis H_1 correspond to the presence of a constant voltage m . This voltage simply shifts the scale, so that

$$p_{r_i|H_1} = \mathcal{F}(r_i - m; \mu, \sigma, \lambda, f) \quad (\text{A.8})$$

Thus the likelihood ratio Λ is

$$\Lambda = \frac{\prod \mathcal{F}(r_i - m)}{\prod \mathcal{F}(r_i)} \quad (\text{A.9})$$

or, equivalently,

$$\log(\Lambda) = \sum \log(\mathcal{F}(r_i - m)) - \sum \log(\mathcal{F}(r_i)) \quad (\text{A.10})$$

Note that the parameters f and λ may be estimated independently of σ , μ and m by monitoring a small sample of the detector array which is kept outside the field of view of the telescope.

A.2 ILLUSTRATIVE EXAMPLE AND COMPARISON WITH SATDI

In this section, we will consider a particular case corresponding to detection against a bright, i.e., nuclear-induced background using IBC detectors. The parameters are

Parameter	Value
TDI	8 stages
μ	400000 electrons
σ	632 ($= \sqrt{\mu}$)
λ	1/4000
f	0.3

The probability density function corresponding to equation A.4 is shown in Figure A-1. It is characterized by a Gaussian part, which falls off rapidly, and a long exponential tail resulting from the γ -induced corruption. In Figure A-2 the log of the likelihood ratio (Equation A.10) is plotted for 3 cases: no γ contamination, 15 percent γ s, and 30 percent γ s. The signal strength m is taken to be 1265 electrons, corresponding to twice the standard deviation of the background noise. The output signal-to-noise ratio is thus $2\sqrt{8}$ or roughly 5.7.

103581-16

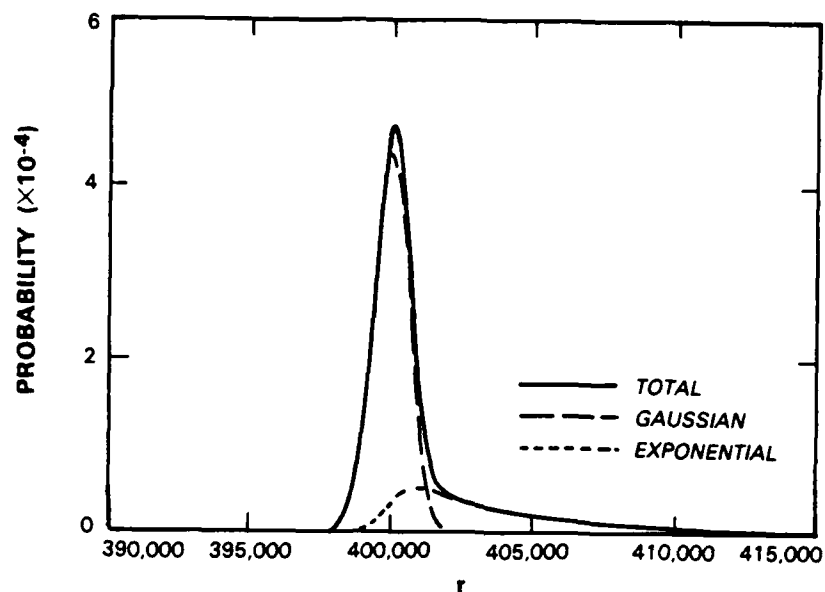


Figure A-1. Probability density function.

103581-17

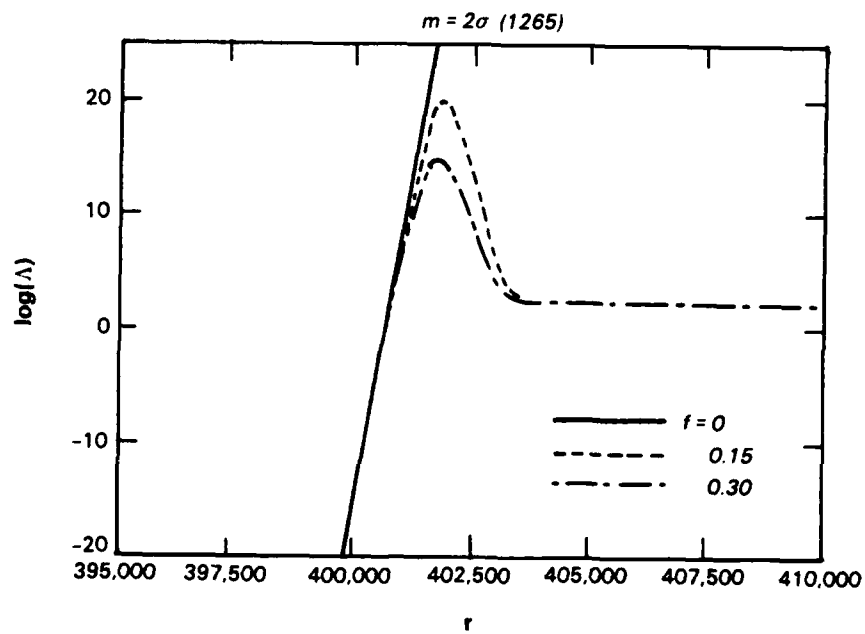


Figure A-2. Log likelihood ratio.

For the γ -free case, the log likelihood ratio is just a straight line, reflecting the classical result for a signal in the presence of Gaussian noise. Addition of γ contamination results in the ratio peaking, then falling back to an asymptote. Physically, this behavior can be thought of as reflecting the fact that high received signals are most likely due to γ contamination. The signals of interest to the detector would thus be those lying in a roughly parabolic region whose bottom is defined by the number of acceptable false alarms.

In contrast, the effect of SATDI is approximately equivalent to taking the $f = 0$ curve and cutting it off sharply at some value of r , creating a triangular region of interest.

The log likelihood ratio is a nonlinear equation and is difficult to analyze analytically, while SATDI is, by nature, heuristic. Therefore, we compared them using a Monte Carlo simulation. Events were generated using our model parameters. For the SATDI case, the algorithm used was that designed for the wafer-scale prototype focal plane processor chip. In this algorithm, σ is estimated as the square root of the average TDI signal, and the γ threshold was set at 1.2σ . The remaining signals were then averaged and compared to a detection threshold.

For the maximum likelihood case, the log likelihood of each sample was calculated, and the sum compared to a detection threshold. All other parameters, however, were known and fixed, so that this simulation does not measure the sensitivity of the method to misestimation of f , λ , and μ .

The two methods are compared in Figure A-3 by plotting the receiver operating characteristic (ROC). In an ROC plot, the probability of detection is plotted versus the probability of false alarm. The curves are approximate fits to the data points, which have significant scatter due to the limited number of Monte Carlo throws per point (20,000). A typical error bar is shown for reference. The maximum likelihood curve lies significantly above the SATDI one, indicating that either much better detection for a fixed false alarm rate, or many fewer false alarms for a fixed detection probability may be achieved.

In conclusion, maximum likelihood detection promises to give significantly better performance than SATDI within the framework of our model of γ noise. Further work must be performed to test the validity of the model, as well as to explore its performance in more realistic cases in which the signal, m , is not known a priori. In these cases, m may be estimated as is currently done with maximum likelihood detection grafted on at the end, or a maximum likelihood estimation technique may be feasible as well, resulting in a unified detection and estimation scheme.

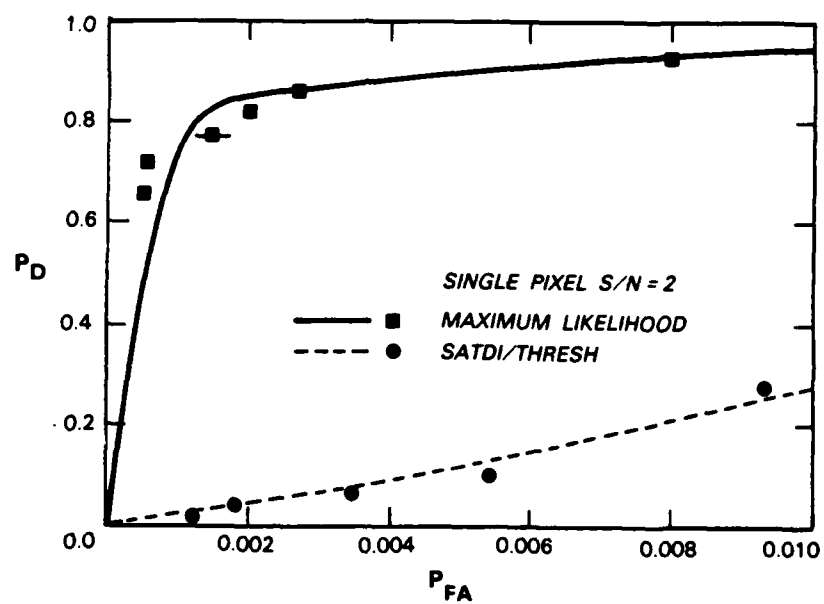


Figure A-3. Receiver operating characteristic.

APPENDIX B ROUNDOFF IN TDI SUMMATION

This Appendix describes a simulation of errors introduced by the proposed TDI summation circuit in the prototype FPP wafer.

The circuit should ideally add the N active TDI inputs ($N \leq 5$) that emerge from gamma circumvention, and then divide the result by N .

Due to implementation constraints, however, the proposed hardware implementation will look like this:

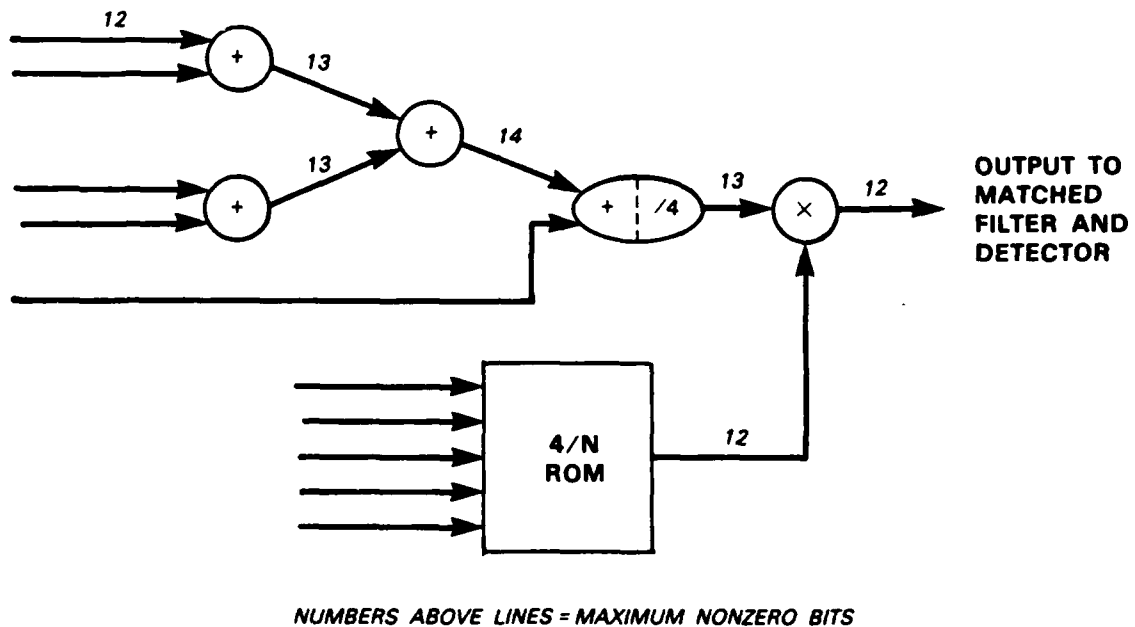


Figure B-1. Detail of proposed TDI summation circuit.

As a consequence, the final result may be off by one bit from the exact method of letting the intermediate sums cascade up to 15 bits.

As might be expected, this effect will be most severe from a percentage point of view when the background level is very low. It is also most noticeable when the γ level is low as well, since when one sample has been rejected due to γ contamination, the above method is exact.

The proposed circuit has been modeled and run through a Monte Carlo program which models the signal and background photons as a Poisson process, and incorporates γ contamination as a random exponential process according to the model of Section 2.5. The circuit was modeled for three cases:

- (1) Low background, high γ : The mean noise level was 35, the signal was 70, and the γ level was 40 percent.
- (2) Low background, low γ : As item (1), but the γ level was 0 percent.
- (3) High background, high γ : The mean noise level was 2000, the signal was 70, and the γ level was 40 percent.

The results are presented in Figures B-2 (a) and (b), and B-3 respectively. The Monte Carlos were generated assuming a 10:1 scaling at the analog to digital converters. (See footnote in Section 2.5.1.) This scale factor is used, for example, in ground-based visible data gathered by Lincoln Laboratory Group 94[11] at the Lincoln Experimental Test System in New Mexico.

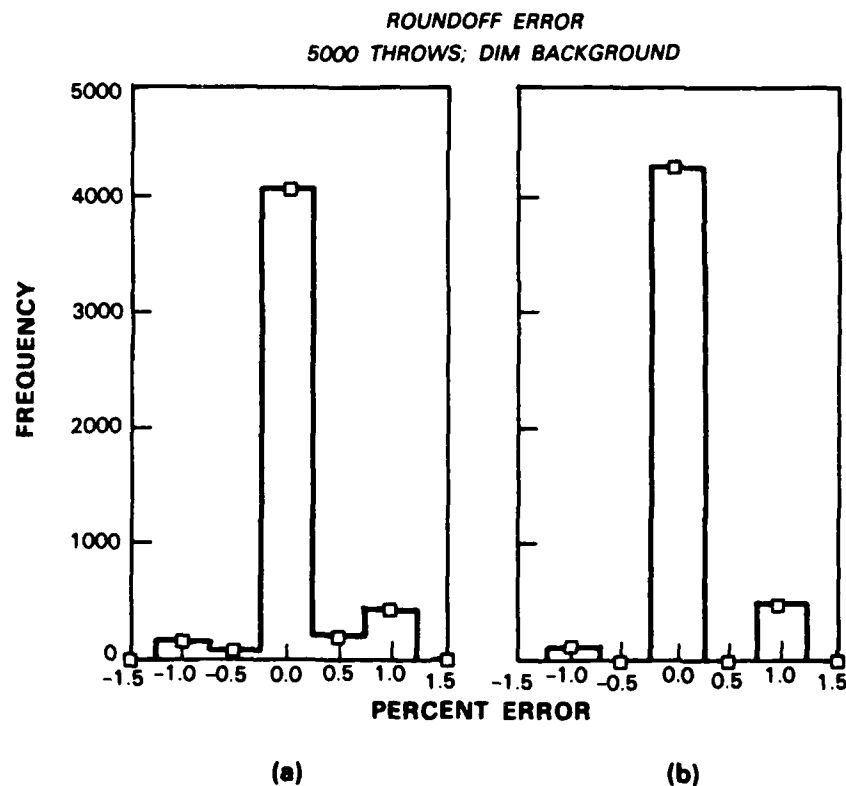


Figure B-2. Low background, (a) high gamma and (b) low gamma simulation.

As expected, the most striking error is in the low background, radiation-free case, where 14 percent of the samples will have errors of ± 1 percent (Figure B-2(b)). The forward bias is due to the Monte Carlo program's practice of always rounding $\frac{1}{2}$ up. A randomized rounding rule will equalize it.

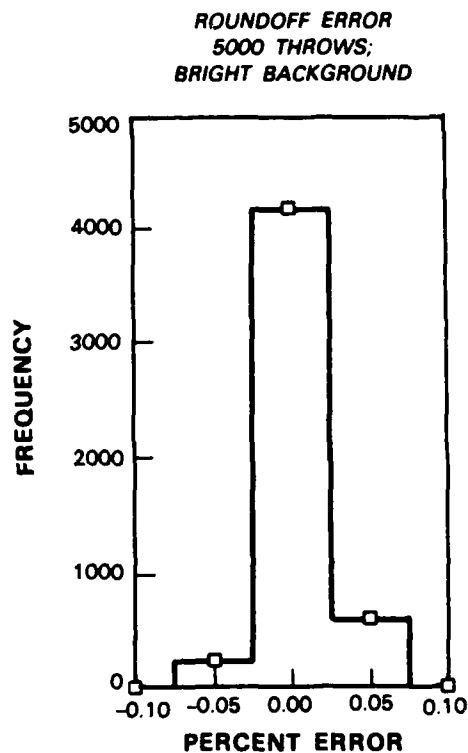


Figure B-3. High background, high gamma simulation.

This behavior is not a serious problem in a prototype processor, but it would have to be addressed in a later, full-up system in which (a) low background observations might be an important part of the mission, or (b) the number of TDI stages is increased.

REFERENCES

1. R. W. Hendrick, Jr., private communication, (1986).
2. E. Segrè, *Nuclei and Particles*, New York: Benjamin (1964).
3. C. E. Woodward, private communication (1988).
4. MIL-HDBK-217E, *Reliability Prediction of Electronic Equipment*, Washington, D.C.: U.S. Department of Defense (1986).
5. L. W. Pinkley, *Sensor Signal Processing Overview*, Huntsville, AL: Nichols Research Corporation (1987).
6. F. M. Rhodes, "Performance Characteristics of the RVLSI Technology" in G. Saucier and J. Trilhe (eds.), *Proc. IFIP WG 10.5 Workshop on Wafer Scale Integration*, (Grenoble, France), Amsterdam: Elsevier (1986).
7. F.M. Rhodes et al., "A Monolithic Hough Transform Processor Based on Restructurable VLSI," in *IEEE Trans. Pattern Anal. Machine Intell.*, 10, No. 1, 106-110, (1988).
8. S. L. Garverick and E. A. Pierce, "A Single Wafer 16-Point 16 MHz FFT Processor," in *Proc. IEEE Custom Integrated Circuits Conf.*, Rochester, NY, 244-248 (1983), DTIC AD-A147514.
9. J. I. Raffel, "The RVLSI Approach to Wafer-Scale Integration," in *Proc. Workshop on Wafer-Scale Integration*, Southampton Univ., England, (1985).
10. B.-Y. Tsaur, "Assessment of Silicon-on-Insulator Technologies for VLSI," in *Semiconductor-On-Insulator and Thin Film Transistor Technology*, Materials Research Society Symposium Proc. v. 53, Pittsburgh, PA, (1986), DTIC AD-A174015.
11. P. L. Chu, private communication, (1987).
12. P. Denyer and D. Renshaw, *VLSI Signal Processing: A Bit-Serial Approach*, Reading, MA: Addison-Wesley, (1985).
13. R. W. Hendrick, Jr., private communication (1987).
14. H. L. Van Trees, *Detection, Estimation and Modulation Theory, Part I*, New York: Wiley (1968).
15. K. H. Norsworthy, R. N. Murata, and T. Tibbetts, "Mosaic Signal Processing in Nuclear Environments," Final Report D180-28537-1, Boeing AeroSpace Company (1984).
16. K. H. Norsworthy, R. N. Murata, and B. E. Northon, "Nuclear Induced Noise Mitigation", Technical Report 2-3774-000-181, Boeing AeroSpace Company (1985).

UNCLASSIFIED

SECURITY CLASSIFICATION OF THIS PAGE

REPORT DOCUMENTATION PAGE

1a. REPORT SECURITY CLASSIFICATION Unclassified			1b. RESTRICTIVE MARKINGS		
2a. SECURITY CLASSIFICATION AUTHORITY			3. DISTRIBUTION/AVAILABILITY OF REPORT Approved for public release; distribution unlimited.		
2b. DECLASSIFICATION/DOWNGRADING SCHEDULE					
4. PERFORMING ORGANIZATION REPORT NUMBER(S) Technical Report 814			5. MONITORING ORGANIZATION REPORT NUMBER(S) ESD-TR-88-173		
6a. NAME OF PERFORMING ORGANIZATION Lincoln Laboratory, MIT		6b. OFFICE SYMBOL (If applicable)		7a. NAME OF MONITORING ORGANIZATION Electronic Systems Division	
6c. ADDRESS (City, State, and Zip Code) P.O. Box 73 Lexington, MA 02173-0073			7b. ADDRESS (City, State, and Zip Code) Hanscom AFB, MA 01731		
8a. NAME OF FUNDING/SPONSORING ORGANIZATION Air Force Space Technology Center		8b. OFFICE SYMBOL (If applicable)		9. PROCUREMENT INSTRUMENT IDENTIFICATION NUMBER F19628-85-C-0002	
8c. ADDRESS (City, State, and Zip Code) Kirtland AFB, NM 87117-6005			10. SOURCE OF FUNDING NUMBERS		
			PROGRAM ELEMENT NO. 63220C	PROJECT NO. 250	WORK UNIT ACCESSION NO.
11. TITLE (Include Security Classification) Design of a Wafer-Scale Focal Plane Processor					
12. PERSONAL AUTHOR(S) Pierre C. Trepagnier					
13a. TYPE OF REPORT Technical Report		13b. TIME COVERED FROM _____ TO _____		14. DATE OF REPORT (Year, Month, Day) 1988, September 15	
15. PAGE COUNT 54					
16. SUPPLEMENTARY NOTATION					
17. COSATI CODES			18. SUBJECT TERMS (Continue on reverse if necessary and identify by block number)		
FIELD	GROUP	SUB-GROUP	focal plane processor, VLSI, wafer-scale architecture, infrared detector, time-dependant processor, fault tolerance, wafer-scale integration, gamma circumvention, image processors		
19. ABSTRACT (Continue on reverse if necessary and identify by block number)					
<p>This report describes a wafer-scale design for an infrared focal plane processor (FPP) to operate in a space environment. The functions of a generic focal plane processor are described, followed by a detailed discussion of a design to be implemented in RVLSI wafer-scale technology for a space-based application. A prototype of this processor (PFPP) will actually be fabricated in rad-hard silicon-on-insulator 3-μm technology. Finally, the question of reliability is explored, and a philosophy of fault tolerance is presented which will lead to a reasonable probability of success over a five-year lifetime.</p> <p><i>wafer-scale include</i></p>					
20. DISTRIBUTION/AVAILABILITY OF ABSTRACT <input type="checkbox"/> UNCLASSIFIED/UNLIMITED <input checked="" type="checkbox"/> SAME AS RPT. <input type="checkbox"/> DTIC USERS			21. ABSTRACT SECURITY CLASSIFICATION Unclassified		
22a. NAME OF RESPONSIBLE INDIVIDUAL Lt. Col. Hugh L. Southall, USAF			22b. TELEPHONE (Include Area Code) (617) 981-2330		22c. OFFICE SYMBOL ESD/TML